Colloid Polym Sci (2012) 290:1799–1809
DOI 10.1007/s00396-012-2724-9

ORIGINAL CONTRIBUTION

Brill transition of nylon-6 in electrospun nanofibers

Chi Wang · Shih-Yung Tsou · Hsuan-Sheng Lin

Received: 25 May 2012 / Accepted: 22 June 2012 / Published online: 7 July 2012
© Springer-Verlag 2012

Abstract Electrospun nylon-6 fibers were prepared from its polyelectrolyte solution in formic acid with different concentrtaions. In situ Fourier transform infrared (FTIR), wide-angle X-ray diffraction and small-angle X-ray scattering (SAXS) were performed on the nylon-6 fibers heated to various temperatures until melting. For comparison, stepwise annealing of the solution-cast film having exclusively the α-form was also carried out to elucidate the structural evolution. Our results showed that Brill transition in the electrospun fibers occurs at a lower temperature than that in the solution-cast film due to the crystal size difference. Differential scanning calorimetry heating traces on the as-spun fibers exhibited a unique crystalline phase with a melting temperature of ~235 °C, higher than the equilibrium melting temperature of nylon-6. The content of high melting temperature (HMT) phase increased with increasing nylon-6 concentration; a maximum of 30 % of the fiber crystallinity was reached for fibers obtained from the 22 wt.% solution regardless of the heating rates used. Based on the SAXS and FTIR results, we speculated that the HMT phase is associated with thick α-form crystals developed from the highly oriented nylon-6 chains that are preserved in the skin layer of the as-spun fibers. A plausible mechanism for the formation of the skin/core fiber morphology during electrospinning was proposed.

Keywords Electrospinning · Nylon-6 · Brill transition · Melting

Introduction

Nylon-6 is one of the important polyamides with wide applications ranging from functional fibers, automotive parts and intimate apparel to solid-state electrolyte because of its excellent mechanical properties and thermal stability. When crystallized, nylon-6 exhibits two major crystalline modifications, i.e., the α- and γ-forms. The former is a thermodynamically stable phase and possesses extended zigzag conformation with hydrogen bonds between antiparallel chains, whereas the latter is kinetically favored and has the amide group rotating 60° from the extended planar conformation with hydrogen bonds between parallel chains [1]. Annealing of melt-quenched amorphous film at 100 °C produced the γ-form crystal and further heating at higher temperatures resulted in the $\gamma \rightarrow \alpha$ transformation [2]. However, for the γ form obtained by iodine treatment $\gamma \rightarrow \alpha$ crystal transformation does not occur prior to melting on heating [3]. Thus, the stability of γ form depends on sample treatments. Provided that $\gamma \rightarrow \alpha$ transformation takes place, the mechanism of melting and recrystallization is proposed. After heating a nylon-6 sample with the α-form crystals, Murthy et al. [4] confirmed the appearance of α' form crystals at elevated temperatures, together with the preserved α-form experiencing thermal expansion, on the basis of wide-angle X-ray diffraction (WAXD) curves. The room-temperature α- and high-temperature α'-forms may coexist over a temperature range, and the transformation between the two crystalline forms is not accompanied by significant changes in the amount of crystallinity. The crystal transformation of $\alpha \rightarrow \alpha'$ is thus used to account for the Brill transition of nylon-6, at which the old pair of WAXD peaks at

Electronic supplementary material The online version of this article (doi:10.1007/s00396-012-2724-9) contains supplementary material, which is available to authorized users.

C. Wang (✉) · S.-Y. Tsou · H.-S. Lin
Department of Chemical Engineering,
National Cheng Kung University,
Tainan 701, Taiwan
e-mail: chiwang@mail.ncku.edu.tw

20.5° and 24.0° (using Cu target) are replaced by the new pair of peaks at 21.5° and 23.0°, which is associated with the α' monoclinic lattice [4]. The high-temperature α' crystal is a meta-stable and remains virtually unchanged until the final melting. In addition to WAXD, the Brill transition is also frequently detected and studied by using Fourier transform infrared (FTIR) spectroscopy, which can trace the subtle variation of chain conformation during heating [1, 5].

Electrospinning is a promising technique to obtain polymeric fibers with a sub-micron diameter. Nylon-6 nanofibers have been readily electrospun from solutions with different solvents and its crystalline modification and crystal orientation developed in the fibers have also been studied [6–10]. Previous results were obtained from the neutral solution of nylon-6, and effects of processing variables on the diameter of nylon-6 fibers have been thoroughly discussed. In the as-prepared fibers, the γ-form is the dominant crystalline modification. After long-term holding at high temperatures and cooling to room temperature, the electrospun fibers underwent the $\gamma \rightarrow \alpha$ crystal transformation, attributable to the melting–recrystallization mechanism [7, 9]. As regards the polyelectrolyte solution of nylon-6, we have examined its spinnability in formic acid with different concentrations at various temperatures [11]. In addition, we have also studied the microstructure of the as-spun fibers by means of X-ray diffraction, infrared spectra, and differential scanning calorimetry. By simply increasing the solution concentration, nylon-6 fibers with the exclusive α-form crystal can be prepared [11]. Also altered was the fiber morphology from round in shape to ribbon like. Both crystalline modification and the fiber shape can be manipulated by varying the rates of solvent diffusion and solvent evaporation. Amongst other things, the presence of a unique phase having a high melting temperature (HMT) of 235 °C was evidently detected in the ribbon-like fibers with full α-form crystals. The unique presence of the HMT phase was reported on annealing the constrained nylon-6 yarns to prevent the fiber shrinkage [12]. The elevation of melting temperature was attributed to the entropy reduction of stretched chains by the imposed constrains. It should be noted that no constrains were applied to the present "nonwoven like" electrospun fibers, which ruled out the plausible source of entropy effect. Recently, the HMT phase was also reported in nylon-6/clay nanocomposites produced by annealing under elevated pressure, and the maximum content was 8 % of the total crystallinity [13]. Similar observations of the HMT phase were also reported in the clay-filled nylon-6 nanocomposites subjected to various processing and thermal treatments [14–16]. This abnormal melting peak is proposed to be related to the melting of constrained lamellae induced by intercalated silicate sheets [15] or chain orientation resulting from the interaction of polymer segments with the clay surface [16]. In the absence of added fillers and imposed constrains, however, our electrospun nylon-6 fibers exhibit a large amount of the HMT phase, about 30 % of fiber crystallinity. A recent study on the high-pressure-induced crystallization of nylon-6 film revealed that α-form crystals are produced with melting temperature of 234 °C after being crystallized at 1.2 GPa [17].

Since the melting temperature of HMT phase is higher than the equilibrium melting temperature of nylon-6 crystals, its origin and formation mechanism in the electrospun fibers deserve more attention. In this work, we carried out in situ FTIR and X-ray scattering on the electrospun fibers during stepwise annealing up to its complete crystal melting. For comparison, solution-cast nylon-6 film was also prepared and studied. A plausible formation model for the HMT phase was proposed based on our observations. Emphasis was also given to the possible phase transitions, i.e., $\gamma \rightarrow \alpha$, $\alpha \rightarrow$pseudohexagonal$\rightarrow \alpha'$, or $\alpha \rightarrow \alpha'$, in such a tiny 1-D nanofiber. It was found that thinner lamellae with smaller lateral dimensions were developed in the electrospun fibers than those in the cast film, giving rise to a lower temperature for Brill transition to proceed.

Experimental section

Materials and sample preparation

Nylon-6 pellets were purchased from Polysciences Co. The weight average molecular weight and density were 35,000 g/mol and 1.14 g/cm^3, respectively. Formic acid (FA; purity of 99 vol.%) purchased from Acros Organics Co. was used as a solvent to prepare electrospinning solutions with different nylon-6 concentrations. Our solution rheology studies revealed that the as-prepared solutions exhibited the typical polyelectrolyte characteristics [11], i.e., $\eta_{sp} \sim \phi^{0.5}$ in the semidilute untangled regime, $\eta_{sp} \sim \phi^{1.52}$ in the semidilute entangled regime, and $\eta_{sp} \sim \phi^{3.77}$ in the concentrated regime, where η_{sp} and ϕ are specific viscosity and volume fraction of nylon-6, respectively. The determined entanglement concentration and concentrated concentration were 1 and 6 wt.%, respectively. For the electrospinning process, a needle with an inner and outer diameter of 1.07 and 1.47 mm, respectively, was used as the spinneret. The prepared solutions with different concentrations (6–22 wt.%) were delivered by a syringe pump (Cole-Parmer) to the needle at a controlled flow-rate of 0.3 mL/h. A positive voltage of 20 kV was applied to the spinneret by a high-voltage source (Bertan, 205B) to provide a sufficient electric field for electrospinning. To construct a needle-to-

plate electrode configuration, a steel net (30×30 cm^2) was used as a collector for the electrospun fibers at a fixed tip-to-collector distance of 70 mm. The morphology of as-spun fibers was observed using scanning electron microscope (SEM; Hitachi S4100), and fiber diameters were measured within electron micrographs from a population of ~500 fibers, from which the average fiber diameter (d_f) and the corresponding standard deviation were determined.

Brill transition measurement

To characterize the structural evolution during stepwise heating, fibers electrospun from the 15 and 22 wt.% nylon-6 solutions were used. The morphology of electrospun fibers is shown in Fig. S1 in the Electronic supplementary material (ESM), in which round fibers with a diameter of ~310 nm were obtained from the 15 wt.% solution, whereas ribbon-like fibers with a width of ~2 μm were prepared from the 22 wt.% solution. De-convolution of their corresponding WAXD intensity profiles indicated that the former possessed mixed crystals of 40 % α- and 60 % γ-form, whereas the latter contained exclusively the α-form crystal [11]. For comparison, film samples were prepared by solution casting from the 15 wt.% nylon-6 solution at room temperature. The thickness of the solution-cast film was ~20 μm.

FTIR spectra of samples were obtained by a Perkin-Elmer Spectrum 100 spectrometer with a resolution of 2 cm^{-1} and 64 scans. In situ FTIR spectra of samples during stepwise annealing at different temperatures (T_a) were obtained to reveal the chain conformation change. A Mettler heating stage (FP900) was used for temperature control, and the temperature protocol is shown in Fig. S2 in the ESM. Using the same temperature protocol, in situ WAXD measurements were also conducted at the wiggler beamline BL23A of the National Synchrotron Radiation Research Center (NSRRC) with an 8-keV (wavelength=0.155 nm) beam. Using two linear position-sensitive detectors for data acquisition, the 2θ range for the WAXD data covered the range of 8–34°. Specimens were sealed in Al pans with Kapton windows ca. 2 mm in diameter for the X-ray beam. Small-angle X-ray scattering (SAXS) measurement was carried out at room temperature, and the data were collected by two-dimensional (200×200 mm^2) proportional counters in a master-slave mode. For SAXS, the scattering vector q ($=4\pi \sin\theta/\lambda$, where 2θ is the scattering angle and λ is the wavelength of X-ray) was ranged from 0.1 to 2.0 nm^{-1}. All the X-ray data were corrected for beam fluctuations, sample absorption, and background scattering. Details of the experimental setup and data analysis can be found elsewhere [18]. Thermograms were obtained by using a DSC (Perkin Elmer, DSC7) under a nitrogen atmosphere at a scanning rate of 10 °C/min, unless specified elsewhere. For the melting endotherm obtained, the peak temperature (T_m) and enthalpy (ΔH_m) were recorded.

Results and discussion

Effects of nylon-6 concentration on the fiber diameter

The pioneering work by McKee et al. pointed out the importance of chain entanglements in forming the electrospun fibers [19]. In the absence of chain entanglements in the electrospinning solution, only spherical particles without fiber-like structure are generated. For the present polyelectrolyte nylon-6/FA solution, the entanglement concentration was determined to be 1 wt.% [11]. However, the minimum concentration required to obtain bead-free fibers was found to be 8 % (Fig. 1). The diameter of electrospun fibers (d_f) increases with increasing solution concentration, ϕ (or zero-shear viscosity, η_o). Nylon-6 fibers with a diameter of 103±

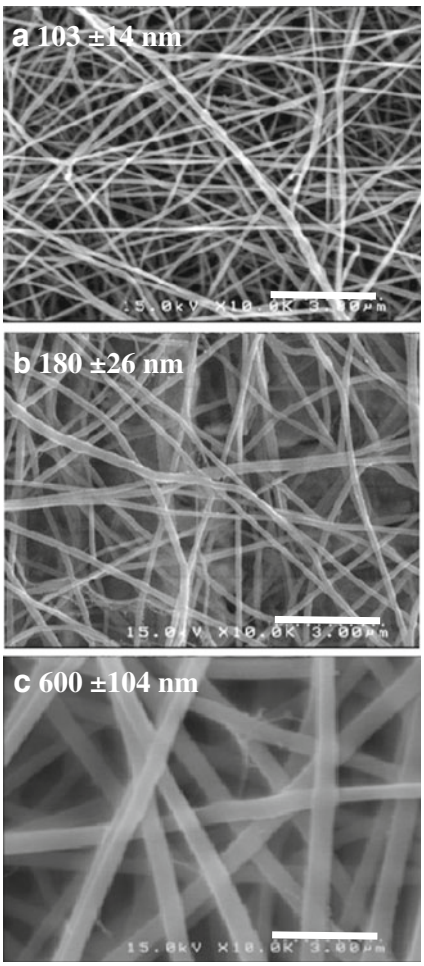

Fig. 1 SEM images of nylon-6 fibers electrospun from solutions with different concentrations of **a** 8, **b** 12, and **c** 18 wt.%. The *scale bar* is 3 μm. The average fiber diameters are displayed

14 nm are obtained from the 8 wt.% solution, whereas 20 wt.% solution yields fibers with a diameter of 855± 215 nm. Based on the uniform fibers obtained from the 8–20 wt.% solutions (Fig. 2), the concentration dependence of d_f is scaled to be: $d_f \sim (\phi/\phi_e)^{2.36}$ and $d_f \sim \eta_o^{0.60}$, where ϕ_e is the entanglement concentration. Similar exponents have been reported either in the neutral solutions of poly(ethylene terephthalate) copolymers [19] and poly(methyl methacrylate) [20] or other polyelectrolyte solution of poly(2-(dimethylamino) ethyl methacrylate hydrochloride) [21]. In other words, there is no significant difference in the derived exponents for the neutral and polyelectrolyte solutions since the concentration of the later required to obtain bead-free fibers is sufficiently high (about 8 ϕ_e) that polyelectrolyte character is screened. Our previous paper [11] showed that the γ-form crystal is the dominant modification in the as-spun fibers as the solution concentration is lower than 12 wt.%. Further increase in the nylon-6 concentration to 15 wt.% leads to the formation of mixed α/γ crystals with the content of α-form of 40 %. Eventually, nylon-6 fibers electrospun from the 22 wt.% solution exclusively contain the α-form modification.

Detection of HMT phase in the electrospun nylon-6 fibers

DSC heating traces on the nylon-6 fibers electrospun from solutions with different concentrations are shown in Fig. 3a, together with that for the solution-cast film. The small endothermic hump in the temperature range of 30–100 °C is associated with the removal of residual water in the samples. Electrospun nylon-6 fibers possess higher melting temperatures than the solution-cast film. In contrast with the solution-cast film showing a single melting peak at 220.3 °C, electrospun fibers exhibit multiple melting endotherms. According to the literature [1], the melting temperatures for the γ and α form crystals are ~215 and ~220 °C, respectively. For the 15 wt.% solution-spun fibers, a melting shoulder relevant to the γ-form crystal is seen in addition to the main melting peak of the α-form at 224.1 °C. In addition, an unusual high melting temperature phase is observed at 233.7 °C, which is even higher than the equilibrium melting temperature of nylon-6 crystal reported at 232.0 °C [22]. As the electrospinning concentration is increased, the γ-form melting shoulder is gradually diminished and the α-form melting peak becomes sharper. Moreover, the endotherm of HMT phase shifts to higher temperatures and becomes broader. The content of this HMT phase was evaluated by the ratio of melting enthalpy above 230 °C to total ΔH_m measured. With increasing nylon-6 concentration from 12 to 22 wt.% (Fig. 3b), the fiber crystallinity indicated by the ΔH_m remains relatively unchanged, but the amount of HMT phase in the as-spun fiber is increased from 7 to 30 % of the fiber crystallinity. It is worthy of noting that the HMT phase was not detected in nylon-6 fibers electrospun from solutions with a concentration lower than 12 wt.% [11]. For the 22 wt.% solution-spun fibers, the HMT phase has a peak temperature at 239.5 °C and the final crystal melting occurs at 245 °C. The first article to address the presence of HMT phase of nylon-6 appeared three decades ago for the melt-spun fibers, which were under constrains during heating to prevent fiber shrinkage [12]. The enhancement of melting temperature was ascribed to the reduction of entropy change during melting of the constrained fibers. Since no constraints were imposed on our electrospun fibers, a different mechanism should be applied to account for the existence of HMT phase.

Two intriguing questions remained to be resolved: what is the origin for the HMT phase? and where is the location of the HMT phase in the electrospun fibers? To ascertain the nature of the HMT phase, in situ WAXD and SAXS were conducted on fibers annealed step by step to different T_a for tracing any variations of crystalline form and lamellar morphology. As a supplementary tool, in situ FTIR was also performed to reveal the subtle chain conformation.

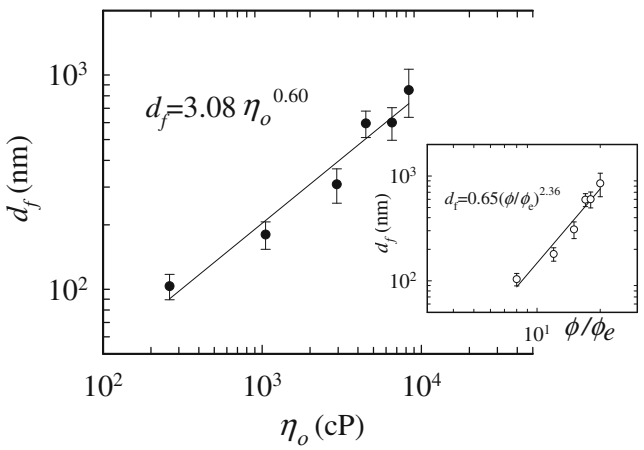

Fig. 2 Solution viscosity dependence of fiber diameter for the nylon-6/FA polyelectrolyte solutions. *Inset* shows the plot of fiber diameter versus the solution concentration (ϕ) normalized with the entanglement concentration (ϕ_e)

Structural variations of nylon-6 in electrospun fiber and cast film during annealing

In situ FTIR spectra at different T_a are displayed in Fig. 4 for fibers electrospun from the 15 and 22 wt.% solutions as well as the solution-cast film. The IR bands at 1,201 and 1,236 cm^{-1} are relevant to the α- and γ-forms, respectively, whereas the 1,292 cm^{-1} band is associated with Brill transition [5]. In agreement with WAXD results [11], the spectrum of 15 wt.% solution-spun fibers indicates coexistence of the α- and γ-forms at 40 °C, but the spectra for fibers obtained from the 22 wt.% solution and cast film exhibit the α-form related band only. Stepwise annealing of the

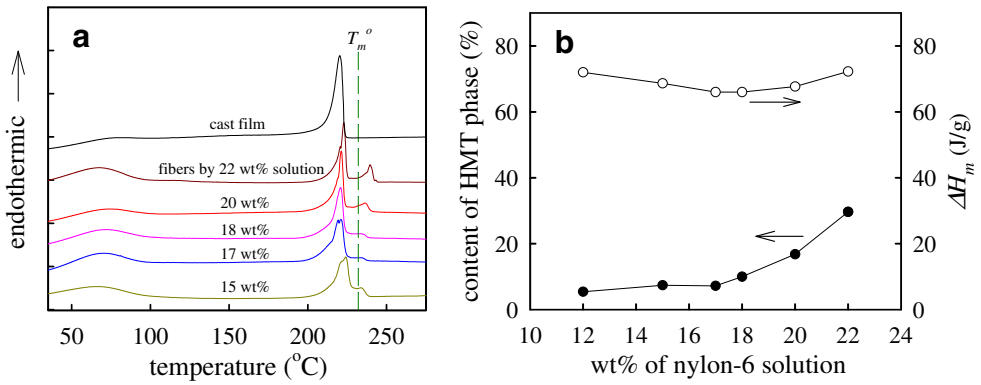

Fig. 3 **a** DSC heating curves of fibers electrospun form nylon-6 solutions with different concentrations. The *dashed line* shows the equilibrium melting temperature of nylon-6 of 232 °C. The heating rate is 10 °C/min. Note the presence of an endothermic hump in the temperature range of 30–100 °C, which is relevant with the removal of residual water in the as-spun fibers. **b** Solution concentration dependence of melting enthalpy and the HMT phase content developed in the as-spun fibers

15 wt.% solution-spun fibers to various T_a leads to the continuous reduction of both 1,201 and 1,236 cm^{-1} bands (Fig. 4a). At 200 °C, a complete melting of the γ-form is observed. The α-related band of 1,201 cm^{-1} is significantly declined at 215 °C and becomes un-detectable at 235 °C plausibly due to the limited amount of the HMT phase (~7 %, Fig. 3b). During the melting of γ-crystal, no abrupt increase of the 1,201 cm^{-1} band is observed, suggesting that there is no $\gamma \rightarrow \alpha$ transformation. Our result is different from that reported by Liu et al. [9] who presented the gradual $\gamma \rightarrow \alpha$ transformation in their nylon-6 fibers electrospun from a volatile solvent of hexafluoro-2-propanol. This discrepancy may suggest that a more volatile solvent used for nylon-6 electrospinning would produce γ crystals with less stability, giving rise to the recrystallization process on heating.

For the 22 wt.% solution-spun fibers (with a HMT phase of ~30 %), with increasing T_a a major reduction of 1,201 cm^{-1} band takes place at 220 °C (Fig. 4b), indicating the melting of α-form. Of particular importance is the detection of the 1,201 cm^{-1} band at 235 °C, which provides the solid evidence that the HMT phase should have the α-form modification. On heating the solution-cast film (Fig. 4c), a progressive intensity reduction of 1,201 cm^{-1} band is seen until 215 °C, at which the α-form crystals completely disappear. It is also noticed that the Brill band disappears at different temperatures for the three samples studied, indicating different structural variations involved during stepwise annealing prior to melting.

WAXD intensity profiles of fibers obtained from the 22 wt.% solution are shown in Fig. 5a. The expanded 2θ range from 18° to 30° is displayed to clearly reveal the WAXD intensity variation. At T_a=30 °C, two WAXD peaks at 2θ=20.5° and 22.9° are observed, and the corresponding *d*-spacing are 0.432 and 0.388 nm, respectively. They are denoted by the α_1 (200) and α_2 (002/202) reflections, which are associated with the inter-chain distance within the H-bonded sheet and the inter-sheet distance, respectively. Upon heating, the α_1 and α_2 reflections move closer to each other and apparently become a broad peak at 160 °C, suggesting the formation of a pseudohexagonal phase [3]. Judging from the full-width of half maximum (FWHM), however, a severe overlapping of two close peaks is likely. As T_a is elevated to 200 °C, the broad peak separates into two with the peak positions at 2θ=21.0° and 22.0°. Further heating to higher T_a results in the reduction of peak intensities without significantly changing the peak positions. These findings imply the appearance of a high-temperature α'-form [3, 4], and the *d*-spacings of α_1' and α_2' reflections are 0.423 and 0.404 nm, respectively. At 230 °C, a weak α_2' reflection is barely seen, plausibly due to the sample flow by the present vertical sample setup and the limited resolution of WAXD. For comparison, the cast film was also stepwise annealed to obtain its corresponding WAXD patterns at various temperatures (Fig. 5b). Solution-cast films possess the α-form crystal, and the diffraction peaks are distinctly sharper than those in Fig. 5a. The width of the diffraction peaks decreases with increasing crystallite size, as suggested by the Scherrer equation. That is, the sharp diffraction peaks correspond to diffraction from large crystallites. On this basis, solution-cast film should possess lamellar crystals with a larger lateral dimension than the electrospun fibers since its FWHM of α_1 and α_2 peaks (2θ=20.4° and 23.6°) are smaller. Upon heating, the α_1 and α_2 peaks move closer to each other with a gradual reduction of the peak intensity. At T_a=200–210 °C, the two WAXD diffraction peaks (α_1' and α_2') are firmly located at 21.0° and 22.0°. At T_a=220 °C, all the crystals are melted away, and only the amorphous halo exists at 2θ=19.8°. We conclude that $\alpha \rightarrow \alpha'$ transformation takes place in the cast film on heating, whereas $\alpha \rightarrow$pseudohexagonal$\rightarrow \alpha'$ transformation occurs in the 22 wt.% solution-spun fibers. In contrast with the cast film, electrospun fibers exhibit the pseudohexagonal phase in the temperature range of 160–180 °C. The variation is attributed to the differences in the crystallization condition. On studying the isothermal crystallization of nylon-6 melt,

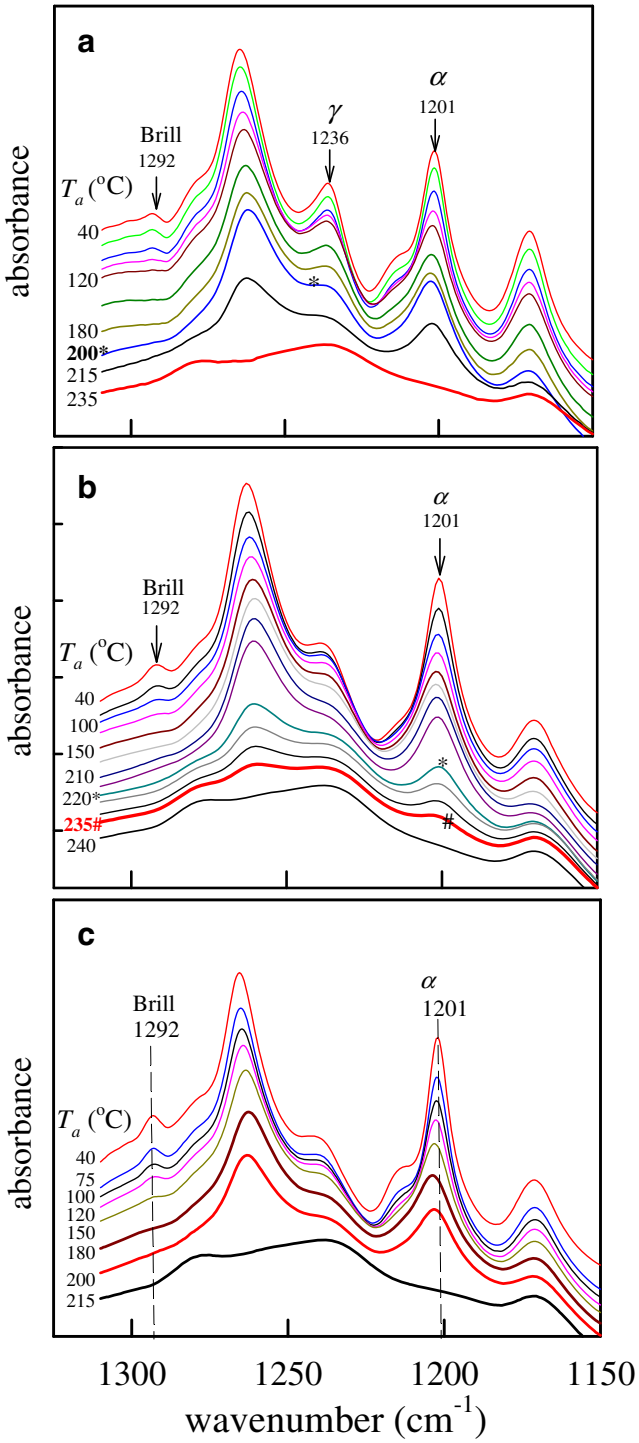

Fig. 4 In situ FTIR spectra of **a** fibers electrospun from 15 wt.% solution, **b** fibers from 22 wt.% solution, and **c** cast film during stepwise annealing at different temperatures, T_a. In (**a**), from *top* to *bottom*: 40, 50, 75, 100, 120, 150, 180, 200, 215, and 235 °C, respectively. The curve at 200 °C is highlighted by an *asterisk* to indicate the complete melting of γ form. In (**b**), from *top* to *bottom*: 40, 75, 100, 120, 150, 180, 210, 215, 220, 225, 230, 235, and 240 °C, respectively. The curves at 220 and 235 °C are highlighted by symbols of *asterisk* and *number sign*, respectively

Ramesh and Gowd [3] found that crystallization temperature plays a major role in the crystal transformation in the film samples. Nylon-6 film crystallized at high temperatures (e.g., 210 °C) exhibited the direct $\alpha \rightarrow \alpha'$ transformation on heating, whereas those crystallized at temperatures lower than 190 °C showed the phase transformation of $\alpha \rightarrow$pseudohexagonal$\rightarrow \alpha'$. The former is similar with our cast film experiencing a slow kinetics for crystallization, and the later is similar with the electrospun fibers crystallized in a fast mode. It seems that the transient pseudohexagonal phase is likely to occur by fast crystallization kinetics.

Displayed in Fig. 6 are the WAXD results for the 15 wt.% solution-spun fibers. The starting fibers possess the mixed crystals of α-form with two reflections at 2θ=20.6° and 22.8°, and of γ-form with one reflection at 2θ=21.4° for the (001) plane. The α_1 and α_2 shoulders become invisible at T_a=100–180 °C. At first glance, one would suggest the disappearance to the completion of α-crystal melting. However, in consideration of the sudden increase in the FWHM of the γ-form (001) reflection, it is more likely that the merging of two small α_1 and α_2 shoulders into the main (001) peak occurs. In other words, the reflections relevant with the α-form are hidden in the (001) reflection of the γ form. This is confirmed by our in-situ FTIR spectra (Fig. 4a), which at this stage show the presence of characteristic α-related bands at 1,201 cm^{-1}. At T_a=200 °C, a significant intensity drop of the (001) reflection is discernible, accompanied by the observation of a small shoulder at 2θ=~22.0°, which is attributed to the α_2' reflection [3, 4]. At T_a=210 °C, traces of γ form (001) and α_2' reflections are detected. At T_a=220 °C, a featureless structure is detected in from the WAXD profile. Based on our FTIR and WAXD results, there is no indication of $\gamma \rightarrow \alpha$ crystal transformation and the γ form can be preserved up to its melting, suggesting the high stability of the γ form in the electrospun fibers. This is consistent with the previous findings from melt-spun fibers [23] or isotropic films produced by iodine treatment [3].

As regards the SAXS profile, Fig. 7 shows the typical Lorentz-corrected intensity plot (Iq^2 versus q) obtained from continuous heating of nylon-6 fibers at a rate of 4 °C/min. Under this heating rate, the corresponding melting temperatures are 223 and 237 °C (see Fig. 10, discussed later). The position of scattering peak (q_m) was used to determine the long period (L) of interlamellar crystallites; $L=2\pi/q_m$. At room temperature, a well defined SAXS peak with a q_m of 0.927 nm^{-1} is observed, corresponding to a long period of 6.8 nm. Upon heating to 120 °C, the position of SAXS peak slightly moves to a lower q and the scattering invariant (Q, the area under the curve) is discernibly increased, due to the removal of residual water in the amorphous layer which

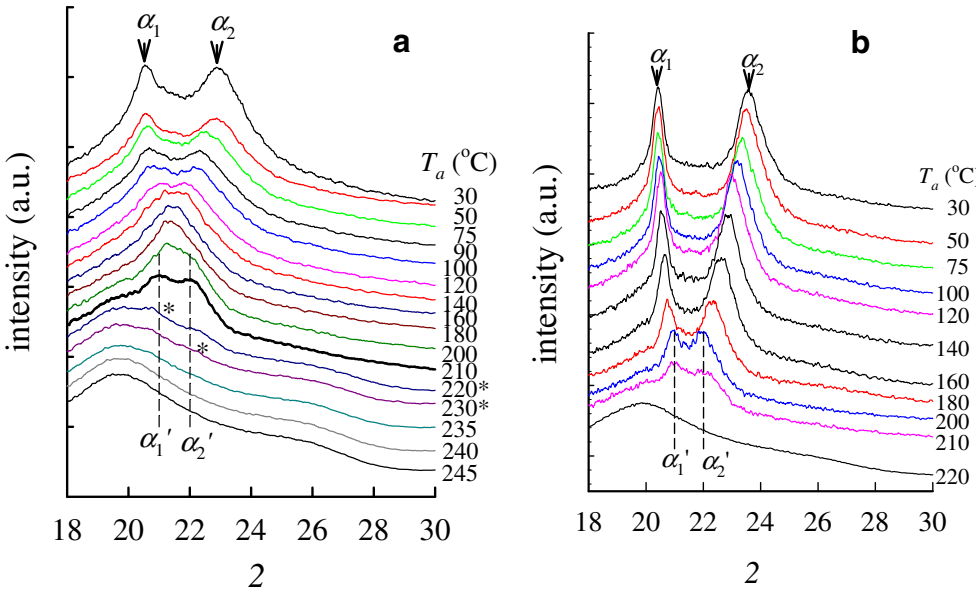

Fig. 5 WAXD intensity profiles of **a** electrospun fibers and, **b** solution-cast film at different temperatures, T_a, during stepwise annealing. The 2θ values for α_1' and α_2' reflections are 21.0° and 22.0°, respectively. The fibers are electrospun from the 22 wt.% nylon-6 solution

enhances the scattering contrast. At T_a higher than 150 °C, the scattering peak progressively shifts to the low q region, together with a pronounced increase in Q. At T_a=200 °C, the SAXS peak reaches its maximum. Further increases in T_a result in the reduction of peak intensity as well as a continuous peak shifting toward a low q region. It is worthy of noting that an evident SAXS peak is still seen in the temperature range of 225–234 °C, above the main melting peak at 223 °C. It suggests that some residual lamellae with large L can survive at such a high T_a and they should be relevant with the HMT phase, which melts at 237 °C.

The variation of long period during annealing is shown in Fig. 8. In comparison with continuous heating, stepwise annealing of the electrospun fibers displays a similar T_a dependence of L, except that featureless structure is detected at T_a higher than 225 °C (Fig. S3 in the ESM). This is attributable to major crystal melting that the fiber membranes may loss its overall integrity and be likely to flow owing to the vertical sample placement. Thus, limited detection time is available to reveal the trace amount of HMT phase (7–30 % of fiber crystallinity) at high T_a regime. It was noticed that the L in the electrospun fibers is lower than in the cast film. Thus, lamellar crystallites in the as-spun fibers possess a smaller dimension not only in the a- and c-axes (judging from the FWHM of WAXD peaks) but also in the chain axis compared with the lamellae developed in the cast film. During heating, L remains relatively unchanged up to 150 °C and then increases rapidly above

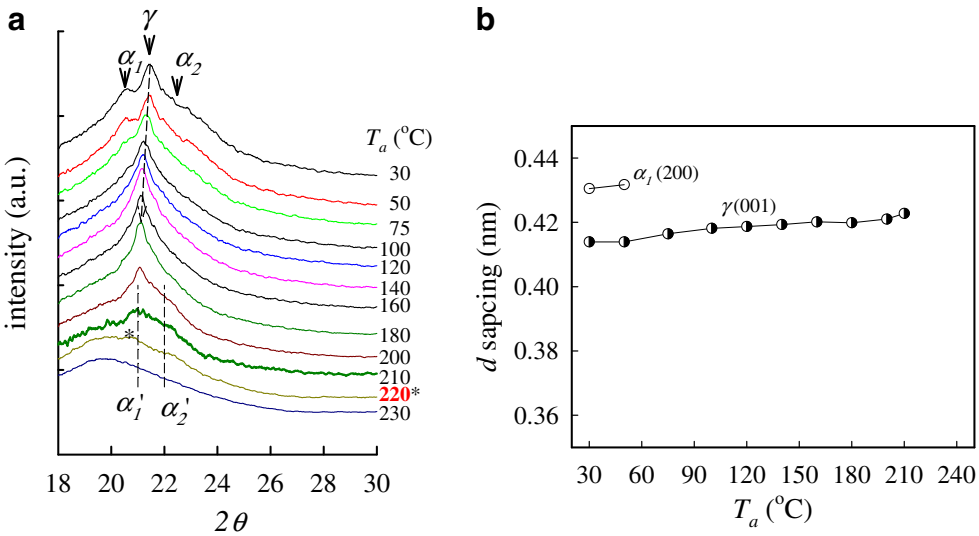

Fig. 6 **a** WAXD intensity profiles electrospun nylon-6 fibers obtained from the 15 wt.% solution at different temperatures, T_a, during stepwise annealing. The 2θ values for α_1' and α_2' reflections are 21.0° and 22.0°, respectively. **b** T_a dependence of d-spacing of the apparent WAXD peaks

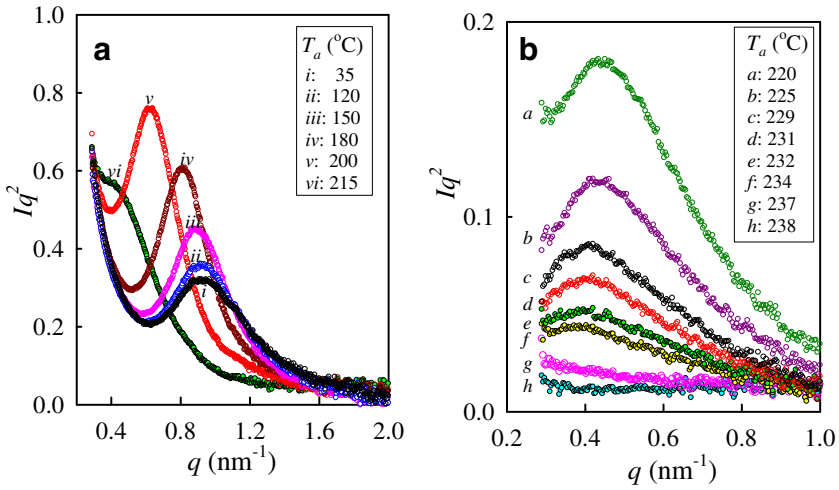

Fig. 7 SAXS patterns collected during continuous heating at 4 °C/min for nylon-6 fibers electrospun from 22 wt.% solution at **a** 35–215 and **b** 220–238 °C. Note the scale difference in *y*-axis between (**a**) and (**b**)

180 °C, suggesting that the nylon-6 lamellae undergo large structural changes above 180 °C. This temperature is much higher than the Brill transition temperature of 150–160 °C (see below). Similar trend is observed for the solution-cast film but the rapid increase in L occurs at 200 °C, at which the Brill transition is completed (see below). The most striking observation is the discontinuity in the change in long period with T_a for the electrospun fibers at 214–224 °C, suggesting the presence of two lamellar populations in the as-spun nylon-6 fibers. Above 225 °C, small amount of nylon-6 lamellae related to the HMT phase exist and its thickness increases with increasing T_a.

Brill transition of nylon-6 in electrospun fibers and cast film

The Brill transition is a feature of even–even nylons. On heating, this type of crystal-to-crystal transition covers a broad temperature range. Conventionally, Brill transition temperature (T_B) is considered as the temperature at which the two WAXD reflections emerge into a single reflection,

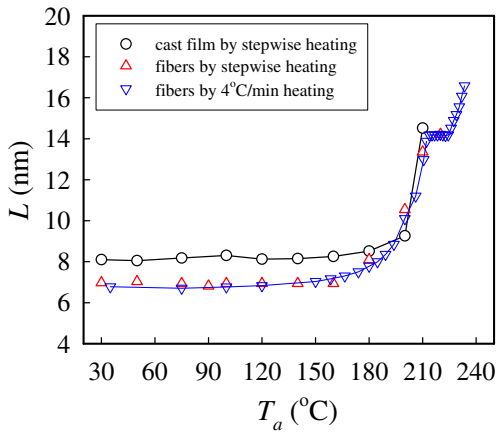

Fig. 8 T_a dependence of long period L for the electrospun fibers and solution-cast film determined from the SAXS intensity profiles

i.e., the formation of pseudohexagonal phase. Brill transition is frequently observed for the nylon-6,6 [24, 25] and nylon-10,10 [26]. For nylon-6, however, the pseudohexagonal phase may not be readily detected since the T_B is too close to its melting temperature. Provided that the pseudohexagonal phase of nylon-6 is absent, the process of $\alpha \rightarrow \alpha'$ transformation is regarded as the Brill transition, as suggested by Murthy et al. [4]. In addition to WAXD, T_B could also be determined from FTIR spectra by the temperature at which the Brill band is vanished. In general, T_B depends strongly upon the crystallization condition [25]; for melt crystallization the higher the crystallization temperature, the higher the observed T_B. In other words, the dimensions and perfection of the nylon crystals both are important in determining the T_B [26].

Figure 9a shows the variations of Brill bands of nylon-6 samples at different T_a. To provide a quantitative analysis, the integrated band area is normalized by that at room temperature. For the solution-cast film, the intensity of the Brill band progressively decreases and becomes null at 180 °C. During Brill transition, the d-spacing variation of nylon-6 crystals is the result of the balance between the thermal expansion and packing tendency of polymer stems within crystals. The variation of d-spacing with T_a is plotted in Fig. 9b, from which T_B can be deduced as well. As the temperature is increased, the 0.442 nm spacing decreases but the 0.372-nm spacing increases. At higher temperatures, two distinct spacings can always be identified, indicating the absence of the pseudohexagonal phase. Thus, the T_B determined from the $\alpha \rightarrow \alpha'$ crystal transition is ~200 °C, which is relatively higher than that (180 °C) derived from FTIR results.

For the fibers electrospun from the 22 wt.% solution, the determined T_B by FTIR is 150 °C and a steep slope is found. As shown in Fig. 9b, the lattice spacings converge to a single reflection at 160 °C (T_B) to form the pseudohexagonal phase, but separate at 200 °C to two reflections having

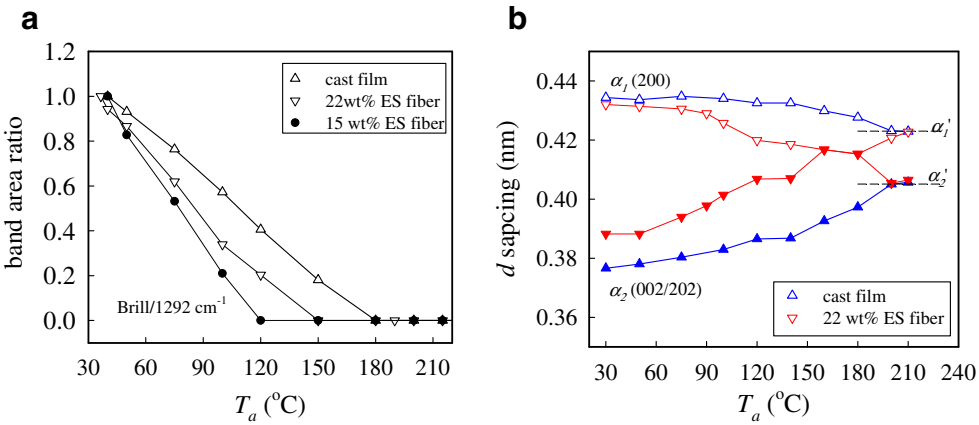

Fig. 9 **a** T_a dependence of the Brill band at 1,292 cm^{-1}. The band area is normalized by that at room temperature. **b** T_a dependence of *d*-spacing of the apparent WAXD peaks

the same *d*-spacings with those of the solution-cast film. Judging from the separation trend of the two *d*-spacings, Brill transition should more readily proceed in the electrospun fibers than in the cast film, in agreement with FTIR results. Within the nylon-6 fibers with mixed α/γ crystals obtained from the 15 wt.% solution, a fast kinetic for Brill transition is observed since the deduced T_B is about 120 °C (Fig. 9a).

Brill transition is a gradual process involving ca. five crystalline stems and not all the stems in the entire crystal. Recent SAXS studies of nylon-10,10 have revealed that the T_B is related to the crystalline dimension [26]. Due to the difference in crystal integrity, larger crystals preserve their original packing order more efficiently to possess a higher T_B, whereas the packing order is more easily re-arranged for smaller crystals, leading to a lower T_B. Based on the WAXD and SAXS results (Figs. 5 and 8), not only the lamellar thickness but also the lateral dimension of nylon-6 crystallites is smaller in the electrospun fibers compared with those in the solution-cast film. These geometric considerations support our findings that Brill transition in the electrospun fibers occurs at a lower temperature than in cast film.

Plausible formation mechanism of HMT phase in electrospun nylon-6 fibers

Figure 10a shows the DSC scans recorded at different heating rates of nylon-6 fibers with pure α-form crystals. Regardless of the heating rates, two major melting peaks were detected in the temperature ranges of 210–230 and 230–245 °C. The former is associated with normal melting of the α-form crystals (denoted as the LMT phase). The HMT phase exhibits two small melting peaks at low heating rates, and possesses a broad peak at high heating rates. Both the melting ranges of LMT and HMT phases are well separated, and no apparent exothermic event is detected between them. The presence of multiple melting peaks is usually attributed to (1) different crystalline modifications, (2) the occurrence of melting, re-crystallization and re-melting, or (3) different lamellar thicknesses and/or

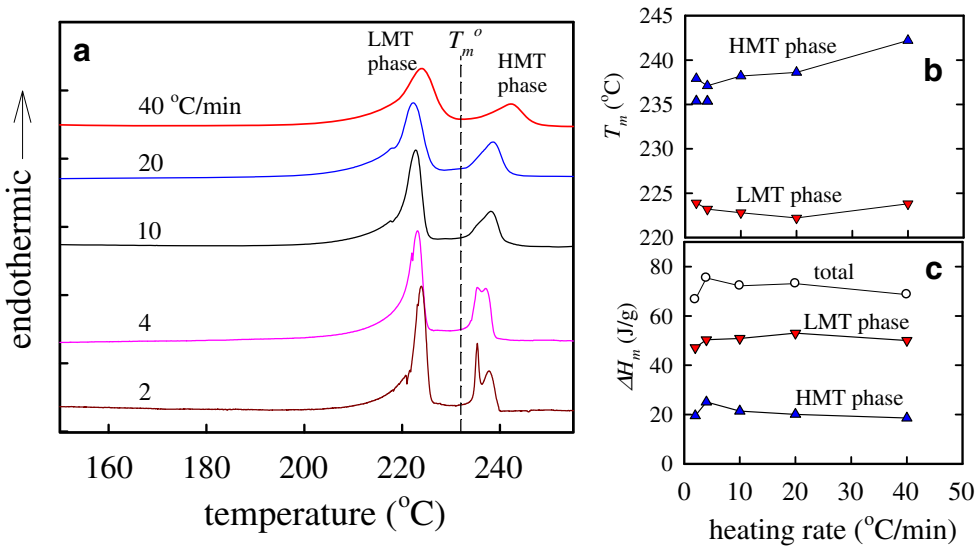

Fig. 10 **a** DSC heating curves of nylon-6 fibers at different heating rates, **b** melting temperature, and **c** melting enthalpy as a function of heating rate. The fibers are obtained from the 22 wt.% nylon-6 solution

crystal perfection. Since no $\alpha \rightarrow \gamma$ crystal transformation takes place during heating, as revealed by the in situ FTIR and WAXD results (Figs. 4b and 5a), the multiple melting behavior cannot be attributed to the presence of different crystalline modifications. As regards the re-crystallization model, this mechanism would be validated provided that the endotherm of the HMT phase is depressed with increasing heating rate. As the heating rate is increased, the melting temperature of the LMT phase remains unchanged at ~223 °C (Fig. 10b), whereas the melting temperature of the HMT phase is increased from 237.9 °C at 2 °C/min to 242.2 °C at 40 °C/min. Moreover, the melting enthalpy of the HMT phase is independent of the heating rate (Fig. 10c). These findings undoubtedly exclude the re-crystallization mechanism, suggesting that the formation of HMT phase is irrelevant with the melting of the LMT phase. The increase in T_m of the HMT phase is attributable to the superheating effect.

Based on the SAXS results (Fig. 8), the HMT phase should be associated with thick nylon-6 crystals with an L of 14–17 nm (with a SAXS peak at a q_m, ~0.4 nm^{-1}). It is remarkable to note that L remained relatively constant at 14.2 nm in the temperature range of 214–224 °C, followed by a rapid increase from 14.5 nm at 225.9 °C to 16.6 nm at 233.5 °C. However, there is no evidence of peak at q values around 0.4 nm^{-1} for temperatures below 200 °C (Fig. 7). It indicates that the as-spun fibers contain no HMT phase, but the LMT phase having the L of ~7 nm. During post-annealing at T_a >200 °C, the HMT phase is gradually induced, plausibly from the highly-oriented chains in the skin layer of the ribbon-like fibers [27]. In other words, we speculate that skin-core morphology is developed in the ribbon-like fibers, and two distinct structures are produced; the fiber core contains the normal nylon-6 lamellae with a melting temperature of ~223 °C (LMT phase), and the skin layer possesses some highly-oriented extended chains which act as the nuclei for the HMT phase during post-annealing.

To thoroughly account for the formation of HMT phase, two issues have to be taken into consideration, i.e., the mechanism to render the skin-core fiber morphology and level of electrical stresses acting on the liquid-gas interface to yield the highly-oriented chains during electrospinning. In general, the cross-sectional structure of electrospun fibers is dependent upon the interplay between the solvent evaporation at the jet surface and solvent diffusion within the liquid jet [28]. A flat profile of polymer concentration along the jet radius leads to the uniform shrinkage of cylindrical jet during drying, eventually producing fibers with a circular cross section, whereas a steep concentration gradient near the jet surface readily results in the skin formation [11, 28, 29], plausibly leading to the ribbon-like fibers [30]. Due to the high conductivity of nylon-6/FA solution, the applied voltage required for the stable cone-jet electrospinning is rather high (above 20 kV), which induces large electrical shear stresses acting on the Taylor-cone surface and jet surface. Liquid motions inside Taylor cone are governed not only by the flow-rate pre-determined by the syringe pump but also the induced electrical stresses, which accelerate the flow of the fluid elements at the cone surface. The tangential electrical stresses drag the surface fluid elements and transport into cone body to a certain thickness. This thin fluid layer possesses a higher velocity than the fluids within the cone body. Thus, nylon-6 chains at the cone surface experience an additional stress to stretch and align themselves during flow towards to the cone apex. When reaching the straight jet region (locating beneath the cone apex), a more significant fluid-element stretching occurs because of the convergent flow due to the cross section reduction. The accelerating flow at the liquid surface not only induces well aligned nylon-6 chains but also enhances the evaporation of FA solvent. Due to the dramatic solvent evaporation, a steep concentration gradient at the liquid-gas interface is developed to readily form a solid skin to lock-in the highly-oriented molecular chains. Enclosed within the solid skin is the remaining liquid core, from which solvent evaporation proceeds. Subsequent drying results in the formation of thin lamellae in the core section.

Conclusions

Brill transition in the electrospun nylon-6 fibers occurs at a temperature lower than that in the solution-cast film. This difference is attributed to the presence of smaller lamellar crystals in the as-spun fiber on the basis of SAXS and WAXD results. A peculiar phase with an unusual melting temperature at ~235 °C is readily found in the ribbon-like nylon-6 fibers. Through the temperature-variable WAXD and SAXS as well as in situ FTIR, we propose that the HMT phase is associated with the thick crystallites developed during post-heating in the skin layer of nylon-6 fibers, which comprises a certain amount of highly oriented molecular chains. The formation of skin-core fiber morphology is attributed the high stretching rate of the conductive solution as well as the enhanced solvent evaporation *at the jet surface* during electrospinning. The former effectively aligns nylon-6 chains in the fluid state, and the latter rapidly locks in the as-developed extended chain conformation. On subsequent annealing, these extended nylon-6 chains serve as the nuclei for the HMT phase. On the other hand, the nylon-6 chains in the core section experience a less electrostatic stretching and undergo moderate kinetics of crystallization to eventually produce normal lamellae with a melting temperature of ~223 °C.

Acknowledgments This work was financially supported by the National Science Council of Taiwan (NSC 98-2221-E-006-005-

MY3, NSC96-2918-I-006-011), National Synchrotron Radiation Research Center (NSRRC, 2009-2-047-5), Taiwan Textile Research Institute (TTRI), and Industrial Technology Research Institute (ITRI). The assistance of X-ray scattering experiments from Drs. U-Ser Jeng and Chun-Jen Su in NSRRC is highly appreciated.

References

1. Murthy NS (2006) Hydrogen bonding, mobility, and structural transitions in aliphatic polyamides. J Polym Sci Polym Phys 44:1763
2. Liu X, Wu Q (2002) Phase transition in nylon 6/clay nanocomposites on annealing. Polymer 43:1933
3. Ramesh C, Gowd EB (2001) High-temperature X-ray diffraction studies on the crystalline transitions in the alpha- and gamma-forms of nylon-6. Macromolecules 34:3308
4. Murthy NS, Curran SA, Aharoni SM, Minor H (1991) Premelting crystalline relaxations and phase-transitions in nylon-6 and 6,6. Macromolecules 24:3215
5. Vasanthan N, Murthy NS, Bray RG (1998) Investigation of Brill transition in nylon 6 and nylon 6,6 by infrared spectroscopy. Macromolecules 31:8433
6. Fong H, Liu W, Wang CS, Vaia RA (2002) Generation of electrospun fibers of nylon 6 and nylon 6-montmorillonite nanocomposite. Polymer 43:775
7. Dersch R, Liu T, Schaper AK, Greiner A, Wendoref JH (2003) Electrospun nanofibers: internal structure and intrinsic orientation. J Polym Sci Polym Chem 41:545
8. Lee KH, Kim KW, Pesapane A, Kim HY, Rabolt JF (2008) Polarized FT-IR study of macroscopically oriented electrospun nylon-6 nanofibers. Macromolecules 41:1494
9. Liu Y, Cui L, Guan F, Gao Y, Hedin NE, Zhu L, Fong H (2007) Crystalline morphology and polymorphic phase transitions in electrospun nylon-6 nanofibers. Macromolecules 40:6283
10. Giller CB, Chase DB, Rabolt JF, Snively CM (2010) Effect of solvent evaporation rate on the crystalline state of electrospun nylon 6. Polymer 51:4225
11. Tsou SY, Lin HS, Wang C (2011) Studies on the electrospun nylon 6 nanofibers from polyelectrolyte solutions: 1. Effects of solution concentration and temperature. Polymer 52:3127
12. Todoki M, Kawaguchi T (1977) Melting of constrained drawn nylon-6 yarns. J Polym Sci Polym Phys 15:1507
13. Kojima Y, Matsuoka T, Takahashi H, Kurauchi T (1994) Crystallization of nylon 6–clay hybrid by annealing under elevated pressures. J Appl Polym Sci 51:683
14. Medellin-Rodriguez FJ, Burger C, Hsiao BS, Chu B, Vaia R, Phillips S (2001) Time-resolved shear behavior of end-tethered nylon 6–clay nanocomposites followed by non-isothermal crystallization. Polymer 42:9015
15. Liu TX, Liu ZH, Ma KX, Shen L, Zeng KY, He CB (2003) Morphology, thermal and mechanical behavior of polyamide 6/layered-silicate nanocomposites. Compo Sci Technol 63:331
16. Winberg P, Eldrup M, Pedersen NJ, van Es MA, Maurer FHJ (2005) Free volume sizes in intercalated polyamide 6/clay nanocomposites. Polymer 46:8239
17. Yu J, Tonpheng B, Andersson O (2010) High-pressure-induced microstructural evolution and enhancement of thermal properties of nylon-6. Macromolecules 43:10512
18. Jeng US, Su CH, Su CJ, Liao KF, Chuang WT, Lai YH, Chang JW, Chen UJ, Huang YS, Lee MT, Yu KL, Lin JM, Liu DG, Chang CF, Liu CY, Chang CH, Liang KS (2010) A small/wide-angle X-ray scattering instrument for structural characterization of air–liquid interfaces, thin films and bulk specimens. J Appl Cryst 43:110
19. McKee MG, Wilkes GL, Colby RH, Long TE (2004) Correlations of solution rheology with electrospun fiber formation of linear and branched polyesters. Macromolecules 37:1760
20. Shenoy SL, Bates WD, Frisch HL, Wnek GE (2005) Role of chain entanglements on fiber formation during electrospinning of polymer solutions: good solvent, non-specific polymer-polymer interaction limit. Polymer 46:3372
21. McKee MG, Hunley MT, Layman JM, Long TE (2006) Solution rheological behavior and electrospinning of cationic polyelectrolytes. Macromolecules 39:575
22. Wunderlich B (1973) Macromolecular physics, vol 1. Academic, New York, p 389
23. Ibanes C, de Boissieu M, David L, Seguela R (2006) High temperature behaviour of the crystalline phases in unfilled and clay-filled nylon 6 fibers. Polymer 47:5071
24. Murthy NS, Wang ZG, Hsiao BS (1999) Interactions between crystalline and amorphous domains in semicrystalline polymers: small-angle X-ray scattering studies of the Brill transition in nylon 6,6. Macromolecules 32:5594
25. Ramesh C, Keller A, Eltink SJEA (1994) Studies on the crystallization and melting of nylon-6,6. 1. The dependence of the Brill transition on the crystallization temperature. Polymer 35:2483
26. Yang X, Tan S, Li G, Zhou E (2001) Dependence of the Brill transition on the crystal size of nylon 10 10. Macromolecules 34:5936
27. Tosaka M, Yamaguchi K, Tsuji M (2010) Latent orientation in the skin layer of electrospun isotactic polystyrene ultrafine fibers. Polymer 51:547
28. Czaputa K, Brenn G, Meile W (2008) Concentration profiles in drying cylindrical filaments. Heat Mass Transf 45:227
29. Sano Y (2001) Dry behavior of acetate filament in dry spinning. Drying Technol 19:1335
30. Koombhongse S, Liu W, Reneker DH (2001) Flat polymer ribbons and other shapes by electrospinning. J Polym Sci Polym Phys 39:2598